State-to-state energy transfer of NH($X\ ^3\Sigma^-, v=0, J, N$) in collisions with He and N_2

Jan Leo Rinnenthal[a] and Karl-Heinz Gericke
Institut für Physikalische und Theoretische Chemie, Technische Universität Braunschweig, Hans-Sommer-Strasse 10, D-38106 Braunschweig, Germany

(Received 21 September 2000; accepted 6 March 2002)

State-to-state rotational energy transfer of ground state NH($X\ ^3\Sigma^-, v=0, J, N$) in collisions with He and N_2 is studied. A complete inversion between the metastable NH($a\ ^1\Delta$) state and the NH($X\ ^3\Sigma^-$) state is generated via the photodissociation of hydrazoic acid at a wavelength of 266 nm. Single state NH($X\ ^3\Sigma^-, v=0, J, N$) is generated by applying the stimulated emission pumping technique using the strongly forbidden NH($a\ ^1\Delta \rightarrow X\ ^3\Sigma^-$) intercombination transition around 794 nm. The ground state NH($X\ ^3\Sigma^-, v=0, J, N$) distribution is probed with respect to all quantum states using laser induced fluorescence varying delay times and pressures. The collision induced energy transfer between the different rotational and spin levels is extensively studied and two comprehensive sets of rate constants for vibrationally elastic and rotationally inelastic collisions with He and N_2 as collision partners are given which include the effect of multiple collisions. We find propensities for ($\Delta N=0, \Delta i=\pm 1$) and ($\Delta N=\pm 1, \Delta i=0$) transitions where N represents the quantum state for nuclear rotation and i represents the index of the spin component F_i. The rotational relaxation for N_2 as a collision partner occurs on the average three times faster than the rotational relaxation with He as a collision partner. The energy dependence of the transition efficiency for only the nuclear rotational quantum number N obeys an energy-gap law for both He and N_2. © *2002 American Institute of Physics.* [DOI: 10.1063/1.1473662]

I. INTRODUCTION

There is an essential lack of information on the dynamics of rotationally inelastic collisional energy transfer within the $v=0$ manifold of the electronic and vibrational ground state of small molecules like the NH radical. No information about state-to-state energy transfer from higher J states than $J=0,1$ is available. But the electronic and vibrational ground state is the most relevant quantum state for typical chemical processes in nature at temperatures up to about 1000 K because it is the most populated quantum state at these temperatures. The reason for this serious lack of information concerning state-to-state energy transfer within the $v=0$ manifold of the electronic ground state is a preparation problem of these quantum states. Generally, it is not possible to populate a single J state exclusively because the rotational levels are already populated and their population distribution obeys a Boltzmann distribution.

Until now, state-to-state measurements of collision induced energy transfer within the electronic and vibrational ground state have only been performed for the lowest rotational states ($J=0,1$). A state selective preparation of the lowest J states can be achieved by decreasing the rotational temperature in a molecular beam. Experiments like this, especially on the NH radical, were performed by Dagdigian.[1] By the use of a hexapole electric field a further selection of different Λ-levels as well as M_J substates can be achieved.[2] However, state selective preparation of higher J states than $J=1,2$ have only been performed for vibrationally or electronically excited molecules.[3–6]

In order to perform state-to-state studies of collision induced rotational energy transfer of molecules in the electronic and vibrational ground state manifold we introduced a new technique for state selective laser preparation of high J quantum states.[7] This new method is based on two steps. In the first and crucial step the molecules are generated in a metastable excited state exclusively so that a complete inversion is achieved. In the second step, the preparation step, the electronic and vibrational ground state of the molecule is state selectively populated by stimulated emission pumping. In order to perform subsequent state-to-state studies, the generated ground state radicals can be detected with laser induced fluorescence (LIF) as a function of collision numbers. The LIF spectra at different collision numbers contain all the information about the population of all rotational states.

By the use of this preparation technique we performed an extensive study of the collision induced energy flux between the different rotational and spin states of ground state NH($X\ ^3\Sigma^-, v=0, J, N$) radicals colliding with Ne.[8] We published a comprehensive set of state-to-state rate constants for inelastic collisions of NH($X\ ^3\Sigma^-, v=0, J, N$) with Ne up to $N=7$ which includes the effect of multiple collisions. We found a propensity for ($\Delta N=0, \Delta i=\pm 1$) and ($\Delta N=\pm 1, \Delta i=0$) transitions where those transitions which change the spin component and conserve the nuclear rotational quantum number N ($\Delta N=0, \Delta i=\pm 1$) are more effective. We further found a typical dependence of the rate con-

[a]Author to whom correspondence should be addressed; electronic mail: j.rinnenthal@tu-bs.de

stants on the transferred energy which can be described by an energy-gap law (EGL).

The aim of the present work is to understand if the former observations are typical for the NH($X\ ^3\Sigma^-, v=0,J,N$)+X collision system or specific for the NH($X\ ^3\Sigma^-, v=0,J,N$)+Ne system. Thus state-to-state rate constants for two more collision partners, He and N_2, were determined. We chose He as the collision partner because state-to-state rate constants for rotational energy transfer of NH($X\ ^3\Sigma^-, v=0,J,N$) with He can also be calculated theoretically on a very accurate basis. Helium has only two electrons which reduces the calculation time for a potential energy surface (PES) of sufficient accuracy. On the other hand, N_2 was chosen as the collision partner because state-to-state rate constants for collisions with N_2 are relevant for combustion processes when nitrogen-containing fuels are heated before entering the combustion zone because thermal decomposition occurs and produces low molecular weight compounds including NH.[9,10]

II. EXPERIMENT

The detailed experimental setup and the data analysis have already been described in a previous publication.[8] In short, the preparation of the NH($X\ ^3\Sigma^-, v=0,J,N$) ground state radicals is realized in two steps: In the first step a 100% population inversion between the metastable NH($a\ ^1\Delta$) state and the NH($X\ ^3\Sigma^-$) state is generated via 266 nm photolysis of HN_3. In the second step the NH($X\ ^3\Sigma^-, v=0,J,N$) ground state radicals are prepared via stimulated emission pumping using the strongly forbidden NH($a\ ^1\Delta \rightarrow X\ ^3\Sigma^-$) intercombination transition.[11] In a third step the NH($X\ ^3\Sigma^-, v=0,J,N$) radicals are detected via LIF using the strong NH($A\ ^3\Pi \leftarrow X\ ^3\Sigma^-$) transition. A NH($A\ ^3\Pi \leftarrow X\ ^3\Sigma^-$) LIF spectrum contains all information about the population distribution within the NH($X\ ^3\Sigma^-$) state. The preparation of the NH($X\ ^3\Sigma^-, v=0,J,N$) as well as the LIF detection are completely state resolved with respect to the three spin components F_1, F_2, and F_3 which implies that also spin relaxation can be studied.

A necessary condition has to be fulfilled in the experiment: Complete rotational relaxation has to be significantly faster than electronic quenching and radiative decay of NH($a\ ^1\Delta$). If the inversion between the metastable NH($a\ ^1\Delta$) state and the NH($X\ ^3\Sigma^-$) state cannot be maintained for the time period between the generation of the inversion via the photodissociation of HN_3 and the probe of NH($X\ ^3\Sigma^-, v=0,J,N$), the probe signal is distorted by NH($X\ ^3\Sigma^-$) radicals which do not result from rotational relaxation of the initially prepared NH($X\ ^3\Sigma^-, v=0,J,N$) state. We determined the radiative lifetime of NH($a\ ^1\Delta$) in a previous experiment via the saturation intensity of the NH($a\ ^1\Delta \rightarrow X\ ^3\Sigma^-$) intercombination transition to be $\tau \approx 12.5$ s.[11] The radiative decay of NH($a\ ^1\Delta$) is too slow to destroy the inversion during the relevant time scale of several hundred nanoseconds. Similarly, the effect of electronic quenching is not strong enough to destroy the necessary inversion during the relevant time scale, except for electronic quenching by the parent molecule HN_3.[12,13] Consequently, in order to study NH–He and NH–N_2 collisions, the concentration of HN_3 was set to 1/100. At this concentration quenching by HN_3 is sufficiently slow.

HN_3, the precursor of NH, is generated by dropwise adding small amounts of phosphoric acid under vacuum conditions to NaN_3.[14] The only evolving gas is HN_3 which is stored in a glass bulb at a maximum pressure of 1 kPa. The pressure in the glass bulb is monitored by a capacitance pressure transducer (MKS Baratron 221 AHS-D-100). In order to guarantee that NH–HN_3 collisions are rare in comparison to NH–He and NH–N_2 collisions on one hand and the LIF signal is sufficient on the other hand, the stored HN_3 is diluted to a mixing ratio of HN_3:He=HN_3:N_2=1:100 at total pressures between 100 and 1600 Pa in the observation chamber.

The observation chamber is evacuated by an oil diffusion pump reaching a base pressure of 10^{-2} Pa. The total pressure in the observation chamber is monitored by another capacitance pressure transducer (MKS Baratron 221 AHS-D-100).

The generation of the NH($a\ ^1\Delta$) radicals (first step) is performed via the 266 nm photodissociation of HN_3 by a 30 mJ light pulse from a Nd:YAG laser (Continuum Surelite II-10). At this wavelength the NH radical is exclusively produced in its first excited $a\ ^1\Delta$ electronic state. The nascent population distribution of the vibrational levels is known to be $(v=0):(v=1):(v=2)=(1):(0.3):(0.02)$.[15] The mean rotational energy of the nascent NH($a\ ^1\Delta, v=0$) radicals is 700 cm^{-1} and its kinetic energy is 7040 cm^{-1} which corresponds to a velocity of 3320 m/s.[16] However, the relaxed velocity of a NH radical at a temperature of 300 K is about 700 m/s. Consequently, caution must be used for rotational relaxation studies because collisions that also affect the NH translational motion induce a change of the rotational quantum numbers (J,N). Since the scope of this work is the examination of collision induced rotational energy transfer in the absence of translational relaxation, it must be guaranteed that the translational relaxation has already occurred before the ground state NH($X\ ^3\Sigma^-, v=0,J,N$) radicals are prepared by the dump laser pulse. This can easily be achieved by choosing the delay time between photolysis and dump laser pulses that is sufficiently long. Since we determined in Doppler experiments that the translational relaxation is about ten times faster than the rotational relaxation[7,17] an upper limit of this delay time is given by the quenching time of NH($a\ ^1\Delta$).[12,13] For He as a collision partner, we used a delay time of 100 ns. Because electronic quenching of NH($a\ ^1\Delta$) by N_2 is stronger a delay time of 50 ns is the best compromise for the measurements with N_2 as a collision partner.

The completely state selective preparation of the ground state NH($X\ ^3\Sigma^-, v=0,J,N$) radicals (second step) is performed via the strongly forbidden NH($a\ ^1\Delta \rightarrow X\ ^3\Sigma^-$) intercombination transition in the wavelength region from 770 to 830 nm applying the stimulated emission technique. The desired wavelength is supplied by a Nd:YAG laser pumped dye laser (Continuum YG 680, TDL 60, IRP) with a pulse width of typically 7 ns and a pulse energy of 30 mJ. The two laser dyes LDS 765 (760–800 nm) and LDS 821 (795–840 nm)

are used with propylene carbonate and methanol as solvents. A detailed description of the NH($a\ ^1\Delta \rightarrow X\ ^3\Sigma^-$) spectrum can be found in Ref. 11. It consists of nine branches denoted as $^{\Delta N}\Delta J(J)$ where ΔN represents the change of the nuclear rotational quantum number N and ΔJ represents the change of the total angular momentum quantum number J: $^OP(J)$, $^PP(J)$, $^QP(J)$, $^PQ(J)$, $^QQ(J)$, $^RQ(J)$, $^QR(J)$, $^RR(J)$, and $^SR(J)$.[11] The pulse energy of 30 mJ is not sufficient to saturate the transition completely. Therefore the Hönl–London factors[18] have to be used in order to calculate the preparation efficiency of the NH($X\ ^3\Sigma^-, v=0,J,N$) ground state radicals via a certain line of the NH($a\ ^1\Delta \rightarrow X\ ^3\Sigma^-$) spectrum. Not all branches are suitable for a preparation of NH($X\ ^3\Sigma^-, v=0,J,N$). First, the $^QP(J)$, $^QQ(J)$, and $^QR(J)$ branches consist of overlapping lines not allowing a state selective preparation. Furthermore, the Hönl–London factor of the $^OP(J)$ branch is too small for an effective preparation of the ground state NH($X\ ^3\Sigma^-, v=0,J,N$). Finally, it is not possible to prepare the NH($X\ ^3\Sigma^-, v=0,J=0,N=1$) level because no transitions exist to that level, and the NH($X\ ^3\Sigma^-, v=0,J=1,N=2$) state cannot be prepared state selectively because the only possible line for a preparation, namely the $^QR(1)$ line, overlaps with the $^QP(3)$ line. Therefore for the preparation of the F_1 levels, NH($X\ ^3\Sigma^-, v=0,J=N+1,N$), we used $^RQ(J)$ lines, for the preparation of F_2 levels, NH($X\ ^3\Sigma^-, v=0,J=N,N$), we used $^RR(J)$ lines for low J values and $^PP(J)$ lines for high J values, and for the preparation of the F_3 levels, NH($X\ ^3\Sigma^-, v=0,J-N,N$), we used $^PQ(J)$ lines. In total we prepared the following 16 levels:

F_1 levels: $(J=2,N=1),(J=3,N=2),$
$(J=4,N=3),(J=5,N=4),$

F_2 levels: $(J=1,N=1),(J=2,N=2),(J=3,N=3),$
$(J=4,N=4),(J=5,N=5),$
$(J=6,N=6),(J=7,N=7),$

F_3 levels: $(J=2,N=3),(J=3,N=4),(J=4,N=5),$
$(J=5,N=6),(J=6,N=7).$

In a third and last step the detection of the NH($X\ ^3\Sigma^-, v=0,J,N$) radicals is performed by LIF after a certain delay time using the strong NH($A\ ^3\Pi, v=0 \leftarrow X\ ^3\Sigma^-, v=0$) transition ($\tau = 440 \pm 15$ ns).[19] This transition was first observed in 1893 and since then has been the subject of numerous investigations. A multitude of highly accurate experimental data is available today.[20–25] The electronic NH($A\ ^3\Pi \leftarrow X\ ^3\Sigma^-$) transition consists of 27 branches which are denoted as $\Delta J_{i''}(J'')$ for the nine main branches and $^{\Delta N}\Delta J_{i',i''}(J'')$ for the 18 satellite branches where $\Delta N = N' - N''$, $\Delta J = J' - J''$, and i indicates the spin component F_i ($i = N+2-J$). We recorded the spectra in the region 335.5–339 nm and used the branches $Q_2(J)$, $^QP_{21}(J)$, $^QR_{23}(J)$, $^QP_{32}(J)$, $Q_3(J)$ $^OP_{12}(J)$, $^OQ_{13}(J)$, $^OP_{23}(J)$, $P_3(J)$, $^PQ_{23}(J)$, $P_2(J)$, $^PR_{13}(J)$, $P_1(J)$, and $^PQ_{12}(J)$ for the population determination of the rotational levels. All relevant states can be monitored completely state-selective in this region. The desired wavelength region is supplied by an excimer (Radiant Dyes, RD-EXC-200) pumped dye laser (Lambda Physik, FL 3002) with a pulse energy of 2 mJ. The NH($A\ ^3\Pi, v=0 \leftarrow X\ ^3\Sigma^-, v=0$) spectra are recorded under saturated conditions which simplifies the population determination because Hönl–London factors need not be considered and line intensities only depend on the degeneracies of the two involved levels of a transition. All three lasers are aligned parallel to each other. The photolysis laser beam and the probe beam are focused by a 500-mm lens from one side into the observation chamber. The dump laser, which is counterpropagating the photolysis and the probe beams, is focused by a 300-mm lens because the transition probability of the NH($a\ ^1\Delta \rightarrow X\ ^3\Sigma^-$) intercombination transition is very low. The foci of the photolysis beam and the dump beam are most carefully overlapped in order to force as many NH($a\ ^1\Delta$) radicals as possible into the $X\ ^3\Sigma^-$ state. The focus of the probe laser beam ($f = 500$ mm) lies several cm beside the foci of both the photolysis and the dump laser beams. Thus the detection laser beam surrounds the photolysis and the dump beams in their focal region and the fly out of the NH($X\ ^3\Sigma^-$) radicals out of the probe laser beam can be neglected. All laser beams are guided through baffles into the observation chamber in order to reduce the influence of scattered light. Furthermore, all lasers operate at a repetition rate of 10 Hz and are triggered via two coupled trigger generators, a master trigger generator (Stanford Research System DG 535), and a slave trigger generator (homebuilt). The total fluorescence is monitored perpendicular to the laser beams through $f/1$ optics and an interference filter (330 ± 30 nm). A boxcar integrator (Stanford Research System, DG 535) registers, amplifies, and integrates the LIF signal. The boxcar integrator is triggered by the probe laser beam via a photodiode. Finally, a computer records the experimental data for further processing.

III. RESULTS AND DISCUSSION

The population distribution of NH($X\ ^3\Sigma^-, v=0,J,N$) at a certain dump-detection delay time was extracted from the LIF spectra by the following procedure. First a spectrum is calculated for some arbitrary start values of the rotational population. Then it is iteratively optimized by minimizing the least-squares sum of the difference between the calculated and the measured spectrum. This is realized in a C++ program. For every initially prepared quantum state we recorded several NH($A\ ^3\Pi, v=0 \leftarrow X\ ^3\Sigma^-, v=0$) spectra at different pressures and dump-detection delay times. As an example, in Figs. 1 and 2 three LIF spectra for three different total pressures in the observation chamber and the corresponding extracted population distributions are shown. Finally, the obtained population profiles for each rotational level are modeled using smoothing spline functions.

There are a few lines within the specified wavelength region that do not belong to the NH($A\ ^3\Pi, v=0 \leftarrow X\ ^3\Sigma^-, v=0$) transition. These lines result from NH($X\ ^3\Sigma, v=1$) generated by electronic quenching of NH($a\ ^1\Delta$). They are weak but they interfere with the lines resulting from NH($X\ ^3\Sigma, v=0$). Therefore we subtracted the NH($A\ ^3\Pi \leftarrow X\ ^3\Sigma^-$) detection spectrum which is obtained

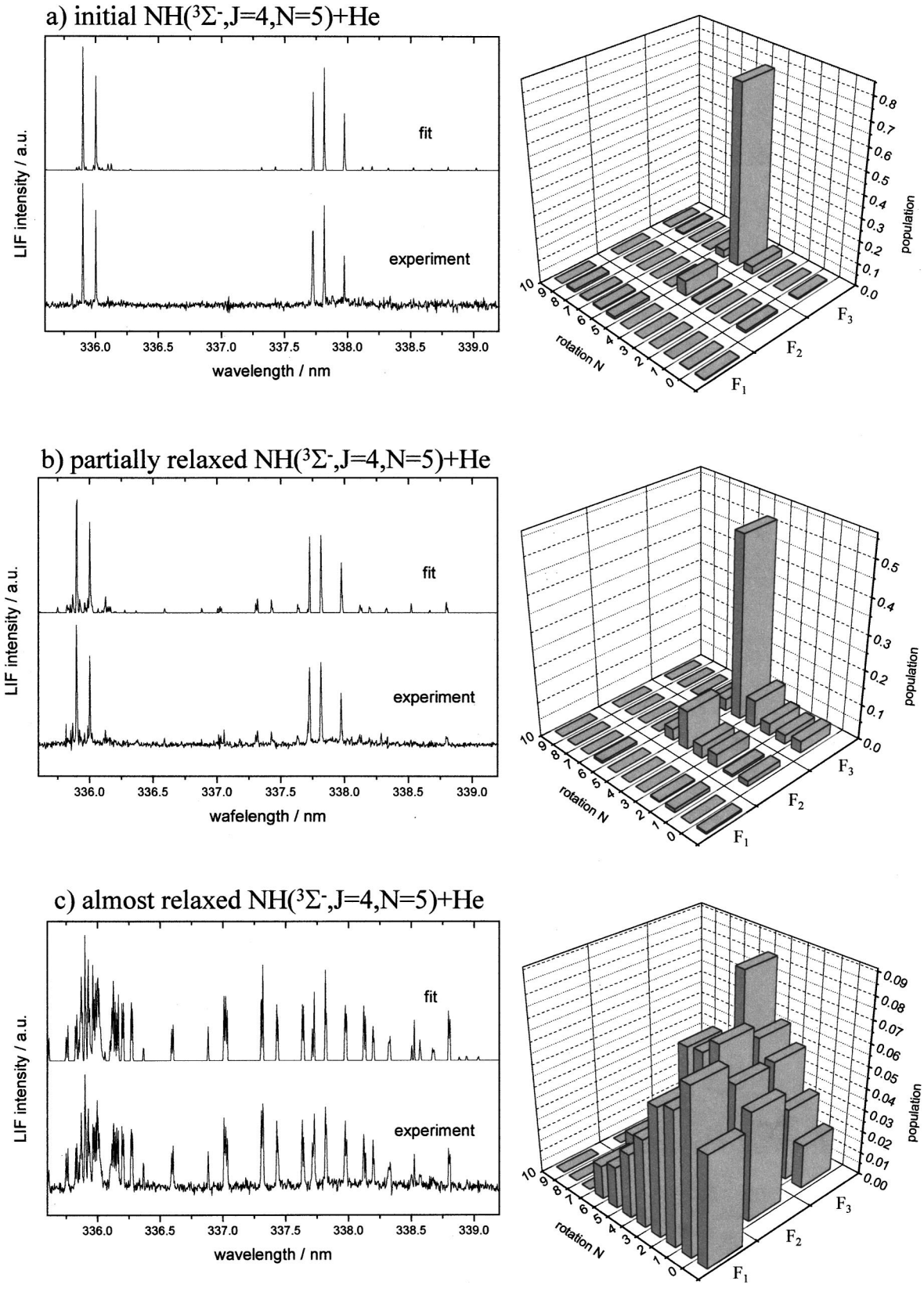

FIG. 1. Monitored and fitted NH($A\ ^3\Pi, v=0 \leftarrow X\ ^3\Sigma^-, v=0$) LIF spectra of NH($X\ ^3\Sigma^-, v=0$)+He where NH($J=4, N=5$) is the initial state which is obtained by scanning the detection laser (left) and the corresponding quantum state populations which are obtained by fitting the spectra (right). The initially prepared quantum state is NH($X\ ^3\Sigma^-, v=0, J=4, N=5$). The mixing ratio is HN_3:He=1:100. The delay time between the photolysis laser pulse and the dump laser pulse is in all cases set to 100 ns. The delay time between the dump laser pulse and the detection laser pulse is set to 50 ns in case (a) and case (b), and 100 ns in case (c). The total pressure in the observation chamber is 100 Pa in case (a), 900 Pa in case (b), and 1600 Pa in case (c). Case (a) represents the nascent situation. Essentially only NH($X\ ^3\Sigma^-, v=0, J=4, N=5$) radicals are present [all lines originate from the single $F_3(J=4, N=5)$ state]. Case (b) represents the situation when the quantum state distribution is partly relaxed by collisions with He. Case (c) represents the situation where the quantum state distribution is almost completely relaxed to a Boltzmann distribution at room temperature.

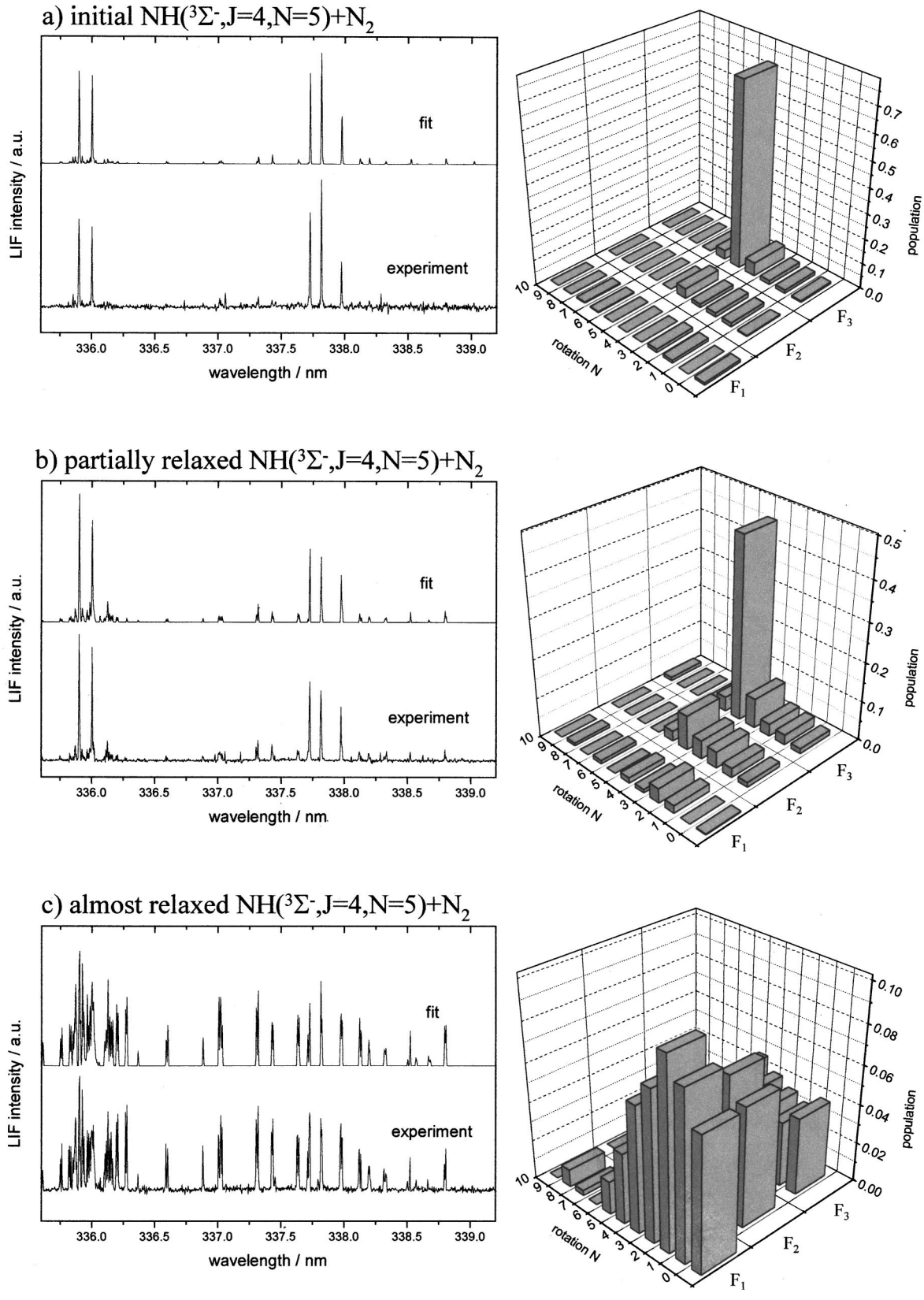

FIG. 2. Monitored and fitted NH($A\ ^3\Pi, v=0 \leftarrow X\ ^3\Sigma^-, v=0$) LIF spectra of NH($X\ ^3\Sigma^-, v=0$)+$N_2$ where NH($J=4, N=5$) is the initial state which is obtained by scanning the detection laser (left) and the corresponding quantum state populations which are obtained by fitting the spectra (right). The mixing ratio is $HN_3:N_2=1:100$. In all cases the delay time between the photolysis laser pulse and the dump laser pulse is set to 50 ns. The delay time between the dump laser pulse and the detection laser pulse is set to 50 ns in case (a) and case (b), and 80 ns in case (c). The total pressure in the observation chamber is 100 Pa in case (a), 300 Pa in case (b), and 700 Pa in case (c). Case (a) represents the nascent situation. Essentially only NH($X\ ^3\Sigma^-, v=0, J=4, N=5$) radicals are present [all lines originate from the single $F_3(J=4, N=5)$ state]. Case (b) represents the situation when the quantum state distribution is partly relaxed by collisions with N_2. Case (c) represents the situation where the quantum state distribution is almost completely relaxed to a Boltzmann distribution at room temperature.

when the dump laser pulse is suppressed from the detection spectrum which is obtained when the dump laser is present. The resulting difference spectrum contains only information about those NH($X\ ^3\Sigma^-, v=0$) radicals only which initially have been prepared with the dump laser pulse. In the experiment the spectra were recorded in two separated channels. Every second pulse of the dump laser is suppressed by a trigger suppressor that inhibits the *Q*-switch of the dump laser system. In addition, the trigger suppressor generates a signal for the computer to indicate in which channel the LIF signal has to be stored.

In order to calculate the state-to-state rate constants for collision induced transitions between the single rotational levels we solve a system of first order coupled differential equations which describes an ensemble of NH ground state radicals which has been prepared at time t_0 by a dump laser pulse in a single NH($X\ ^3\Sigma^-, v=0, J, N$) state, evolving in time:

$$\frac{dP_{J,N}^{J,N}(t)}{dt} = [\mathrm{X}]\left(\sum_{(J',N')\neq(J,N)}^{(J',N')_{\max}} P_{J',N'}^{J,N}(t) k_{\mathrm{X}}^{(J,N)\leftarrow(J',N')} - P_{J,N}^{J,N}(t) \sum_{(J',N')\neq(J,N)}^{(J',N')_{\max}} k_{\mathrm{X}}^{(J,N)\rightarrow(J',N')} \right) + [\mathrm{HN_3}] \times \left(\sum_{(J',N')\neq(J,N)}^{(J',N')_{\max}} P_{J',N'}^{J,N}(t) k_{\mathrm{HN_3}}^{(J,N)\leftarrow(J',N')} - P_{J,N}^{J,N}(t) \sum_{(J',N')\neq(J,N)}^{(J',N')} k_{\mathrm{HN_3}}^{(J,N)\rightarrow(J',N')} \right). \quad (1)$$

Equation (1) describes the initially prepared state. Similar equations hold for all rotational levels. $P_{J,N}^{J,N}(t)$ is the population of the (J,N) state (lower index) at time t for an initial preparation of the same state (upper index). $P_{J',N'}^{J,N}(t)$ is the population of the (J',N') state at time t for an initial preparation of the (J,N) state. $k_{\mathrm{X}}^{(J,N)\leftarrow(J',N')}$ and $k_{\mathrm{X}}^{(J,N)\rightarrow(J',N')}$ are the rate constants for a transition from the (J',N') state to the (J,N) state and vice versa which is caused by a collision with X (X=He or N_2). $k_{\mathrm{HN_3}}^{(J,N)\leftarrow(J',N')}$ and $k_{\mathrm{HN_3}}^{(J,N)\rightarrow(J',N')}$ are the rate constants for HN_3 as a collision partner. [X] is the concentration of the collision partner He or N_2 whereas [HN_3] is the concentration of HN_3, the precursor of NH. The sums extend over all states except the initially prepared state. The first term in the brackets describes the population increase of the (J,N) state by transitions from the neighboring (J',N') states whereas the second term describes the population decrease of the (J,N) state into the (J',N') states. The equations are coupled by the $P_{J',N'}^{J,N}(t)$. In order to predict the time dependent populations of all states $P_{J',N'}^{J,N}(t)$ considered, it is necessary to solve the master equation for given start conditions. These start conditions are the populations of each single state at time t_0, $P_{J',N'}^{J,N}(t_0)$, which are fixed with a pulse of the dump laser in the experiment. Because the preparation of a single NH($X\ ^3\Sigma^-, v=0, J, N$) state with a dump laser pulse is completely state selective we obtain the well-defined start conditions:

$$P_{J',N'}^{J,N}(t_0) = \delta_{(J,N),(J',N')}, \quad (2)$$

where $\delta_{(J,N),(J',N')}=1$ if $(J,N)=(J',N')$ and $\delta_{(J,N),(J',N')}=0$ if $(J,N)\neq(J',N')$. For a solution of the master equation (1) the rate constants $k_{\mathrm{X}}^{(J,N)\leftarrow(J',N')}$, $k_{\mathrm{X}}^{(J,N)\rightarrow(J',N')}$, $k_{\mathrm{HN_3}}^{(J,N)\leftarrow(J',N')}$, and $k_{\mathrm{HN_3}}^{(J,N)\rightarrow(J',N')}$ are needed. For the extraction of the rate constants from the experimental data including the effect of multiple collisions we use an iterative integrated profiles method which is described in detail in a previous publication[8] and is realized as a C program.

Generally, as in our previous study with Ne as the collision partner,[8] we find a propensity for transitions to the neighboring quantum states. In these transitions either the nuclear rotational quantum number N is changed by ±1 or the index of the spin component i is changed by ±1. When the nuclear rotational quantum number N is changed transitions which increase N by 1 are more effective than transitions which decrease N by 1. Transitions between high J states are less effective than transitions between low J states. Transitions which change i by more than ±1 are found to be extremely ineffective.

The complete set of state-to-state rate constants determined in this experiment is presented in Tables I–VIII for He as the collision partner and Tables IX–XVI for N_2 as the collision partner. For the sake of clarity the (J,N) states are denoted as (N,F_i) states where $i=N+2-J$. The initially prepared (N,F_i) states are marked by an asterisk and the rate constants for collision induced transitions into all other states have been determined directly by fitting them in the master equation (1). States which are indicated by a minus sign represent initial states which have not been prepared in the experiment. In this case the rate constants for the collision induced transitions to all other states have been calculated indirectly as described in a previous publication.[8] The accuracy of the values was determined

TABLE I. State-to-state rate constants $k_{\mathrm{He}}^{(J,N)\rightarrow(J',N')}$ in units of 10^{-11} cm^3 molecule^{-1} s^{-1} for collision induced transitions with He as the collision partner. The accuracy of the single rate constants is 0.08 $\times10^{-11}$ cm^3 molecule^{-1} s^{-1}, the accuracy of the sums is 0.4 $\times10^{-11}$ cm^3 molecule^{-1} s^{-1}. The asterisk indicates initial levels which have been prepared in the experiment. All state-to-state rate constants with such an initial level are determined directly. The minus sign indicates initial levels which have not been prepared in the experiment. All rate constants with such an initial level are determined indirectly. The last row contains the sum of all rate constants which originate from the considered level indicated with an asterisk or a minus sign. $F_2(N=0)$ and $F_3(N=0)$ levels do not exist.

Initial $N=0$, F_1 rate constants, collision partner He			
N	F_1	F_2	F_3
0	–		
1	1.70	1.12	0.34
2	2.37	1.11	0.34
3	0.24	0.52	0.11
4	0.12	0.01	0.30
5	0.00	0.00	0.02
6	0.00	0.00	0.00
7	0.00	0.00	0.00
8	0.00	0.00	0.00
	$\Sigma k = 8.30$		

TABLE II. State-to-state rate constants $k_{He}^{(J,N)\to(J',N')}$ in units of 10^{-11} cm^3 molecule^{-1} s^{-1} for collision induced transitions with He as the collision partner. The accuracy of the single rate constants is 0.08 $\times 10^{-11}$ cm^3 molecule^{-1} s^{-1}, the accuracy of the sums is 0.4 $\times 10^{-11}$ cm^3 molecule^{-1} s^{-1}. The asterisk indicates initial levels which have been prepared in the experiment. All state-to-state rate constants with such an initial level are determined directly. The minus sign indicates initial levels which have not been prepared in the experiment. All rate constants with such an initial level are determined indirectly. The last row contains the sum of all rate constants which originate from the considered level indicated with an asterisk or a minus sign. $F_2(N=0)$ and $F_3(N=0)$ levels do not exist.

	Initial $N=1$ rate constants, collision partner He								
	Initial $N=1$, F_1			Initial $N=1$, F_2			Initial $N=1$, F_3		
N	F_1	F_2	F_3	F_1	F_2	F_3	F_1	F_2	F_3
0	1.19			1.31			1.19		
1	*	2.28	1.58	3.55	*	0.15	7.86	0.44	−
2	2.40	0.83	0.31	0.85	3.18	0.63	3.18	0.79	2.12
3	1.81	0.86	0.23	0.44	1.33	0.37	2.38	1.34	1.18
4	0.65	0.13	0.19	0.09	0.13	0.21	0.07	0.64	2.17
5	0.05	0.11	0.04	0.00	0.18	0.01	0.00	0.31	0.56
6	0.13	0.04	0.00	0.00	0.00	0.01	0.00	0.02	0.19
7	0.06	0.01	0.04	0.06	0.00	0.04	0.00	0.00	0.04
8	0.03	0.03	0.01	0.09	0.03	0.00	0.00	0.00	0.00
	$\Sigma k=13.01$			$\Sigma k=12.66$			$\Sigma k=24.48$		

TABLE IV. State-to-state rate constants $k_{He}^{(J,N)\to(J',N')}$ in units of 10^{-11} cm^3 molecule^{-1} s^{-1} for collision induced transitions with He as the collision partner. The accuracy of the single rate constants is 0.08 $\times 10^{-11}$ cm^3 molecule^{-1} s^{-1}, the accuracy of the sums is 0.4 $\times 10^{-11}$ cm^3 molecule^{-1} s^{-1}. The asterisk indicates initial levels which have been prepared in the experiment. All state-to-state rate constants with such an initial level are determined directly. The minus sign indicates initial levels which have not been prepared in the experiment. All rate constants with such an initial level are determined indirectly. The last row contains the sum of all rate constants which originate from the considered level indicated with an asterisk or a minus sign. $F_2(N=0)$ and $F_3(N=0)$ levels do not exist.

	Initial $N=3$ rate constants, collision partner He								
	Initial $N=3$, F_1			Initial $N=3$, F_2			Initial $N=3$, F_3		
N	F_1	F_2	F_3	F_1	F_2	F_3	F_1	F_2	F_3
0	0.21			0.57			0.17		
1	1.32	0.51	0.58	0.86	1.21	0.42	0.19	0.64	0.52
2	1.83	0.56	0.09	1.25	1.85	0.09	0.25	0.92	0.77
3	*	1.50	0.03	1.72	*	1.61	0.24	3.46	*
4	1.37	0.33	0.04	0.08	1.54	0.96	0.13	0.22	1.83
5	0.36	0.34	0.04	0.05	0.35	0.11	0.01	0.13	0.31
6	0.17	0.07	0.00	0.06	0.16	0.15	0.00	0.00	0.14
7	0.10	0.00	0.13	0.09	0.00	0.02	0.00	0.00	0.01
8	0.02	0.02	0.00	0.05	0.05	0.00	0.09	0.01	0.00
	$\Sigma k=9.62$			$\Sigma k=13.25$			$\Sigma k=10.04$		

to be 0.08×10^{-11} cm^3 molecule^{-1} s^{-1} for the rate constants with He as the collision partner and 0.25×10^{-11} cm^3 molecule^{-1} s^{-1} for the rate constants with N_2 as the collision partner by a linear fit in the $t\approx t_0$ regime [Eq. (3) in Ref. 7].

In the last row of each table the total rate constant for collision induced transitions out of the initial level is listed (the decrease of the initially prepared state), which represents the sum over all other rate constants. Figure 3 represents the dependence on N of the total rate constants for the F_1, F_2, and F_3 levels as initial levels for He (above) and N_2 (below) as the collision partners. Also shown are the mean total rate constants averaged over the initial i. Generally, the total rate constant decreases with increasing N, as can be seen very clearly for the mean total rate constants. The total rate constants for He as the collision partner with F_3 levels as initial levels have the strongest decrease with N if we look at the slope, $\Delta(\Sigma k)/\Delta N$, of a linear regression fit [$\Delta(\Sigma k)/\Delta N=$

TABLE III. State-to-state rate constants $k_{He}^{(J,N)\to(J',N')}$ in units of 10^{-11} cm^3 molecule^{-1} s^{-1} for collision induced transitions with He as the collision partner. The accuracy of the single rate constants is 0.08 $\times 10^{-11}$ cm^3 molecule^{-1} s^{-1}, the accuracy of the sums is 0.4 $\times 10^{-11}$ cm^3 molecule^{-1} s^{-1}. The asterisk indicates initial levels which have been prepared in the experiment. All state-to-state rate constants with such an initial level are determined directly. The minus sign indicates initial levels which have not been prepared in the experiment. All rate constants with such an initial level are determined indirectly. The last row contains the sum of all rate constants which originate from the considered level indicated with an asterisk or a minus sign. $F_2(N=0)$ and $F_3(N=0)$ levels do not exist.

	Initial $N=2$ rate constants, collision partner He								
	Initial $N=2$, F_1			Initial $N=2$, F_2			Initial $N=2$, F_3		
N	F_1	F_2	F_3	F_1	F_2	F_3	F_1	F_2	F_3
0	1.62			1.07			0.54		
1	2.12	0.39	0.62	1.08	1.76	0.22	0.71	0.86	0.97
2	*	2.73	0.30	5.59	*	1.98	0.71	3.29	−
3	2.64	0.52	0.19	0.57	3.55	1.28	0.17	0.13	0.80
4	0.87	0.57	0.16	0.55	1.56	0.74	0.16	0.15	0.54
5	0.19	0.21	0.14	0.15	0.44	0.13	0.00	0.00	0.05
6	0.01	0.01	0.00	0.02	0.01	0.00	0.00	0.00	0.09
7	0.01	0.00	0.01	0.01	0.00	0.01	0.00	0.00	0.01
8	0.04	0.00	0.02	0.01	0.00	0.00	0.00	0.00	0.00
	$\Sigma k=13.37$			$\Sigma k=20.73$			$\Sigma k=9.18$		

TABLE V. State-to-state rate constants $k_{He}^{(J,N)\to(J',N')}$ in units of 10^{-11} cm^3 molecule^{-1} s^{-1} for collision induced transitions with He as the collision partner. The accuracy of the single rate constants is 0.08 $\times 10^{-11}$ cm^3 molecule^{-1} s^{-1}, the accuracy of the sums is 0.4 $\times 10^{-11}$ cm^3 molecule^{-1} s^{-1}. The asterisk indicates initial levels which have been prepared in the experiment. All state-to-state rate constants with such an initial level are determined directly. The minus sign indicates initial levels which have not been prepared in the experiment. All rate constants with such an initial level are determined indirectly. The last row contains the sum of all rate constants which originate from the considered level indicated with an asterisk or a minus sign. $F_2(N=0)$ and $F_3(N=0)$ levels do not exist.

	Initial $N=4$ rate constants, collision partner He								
	Initial $N=4$, F_1			Initial $N=4$, F_2			Initial $N=4$, F_3		
N	F_1	F_2	F_3	F_1	F_2	F_3	F_1	F_2	F_3
0	0.16			0.02			0.62		
1	0.13	0.01	0.01	0.27	0.18	0.92	0.52	0.55	1.27
2	1.52	0.11	0.13	0.47	1.09	0.15	0.36	0.34	0.69
3	1.50	0.36	0.09	0.83	1.69	0.12	1.18	2.09	1.73
4	*	1.90	0.05	1.56	*	2.70	1.24	3.42	*
5	1.35	0.59	0.00	0.37	1.05	0.94	0.05	0.30	1.35
6	0.00	0.18	0.02	0.11	0.00	0.14	0.05	0.00	0.17
7	0.04	0.07	0.07	0.18	0.00	0.06	0.10	0.00	0.11
8	0.15	0.00	0.00	0.02	0.00	0.03	0.08	0.00	0.06
	$\Sigma k=8.44$			$\Sigma k=12.90$			$\Sigma k=16.28$		

TABLE VI. State-to-state rate constants $k_{He}^{(J,N)\to(J',N')}$ in units of 10^{-11} cm^3 molecule^{-1} s^{-1} for collision induced transitions with He as the collision partner. The accuracy of the single rate constants is 0.08 $\times 10^{-11}$ cm^3 molecule^{-1} s^{-1}, the accuracy of the sums is 0.4 $\times 10^{-11}$ cm^3 molecule^{-1} s^{-1}. The asterisk indicates initial levels which have been prepared in the experiment. All state-to-state rate constants with such an initial level are determined directly. The minus sign indicates initial levels which have not been prepared in the experiment. All rate constants with such an initial level are determined indirectly. The last row contains the sum of all rate constants which originate from the considered level indicated with an asterisk or a minus sign. $F_2(N=0)$ and $F_3(N=0)$ levels do not exist.

	Initial $N=5$ rate constants, collision partner He								
	Initial $N=5$, F_1			Initial $N=5$, F_2			Initial $N=5$, F_3		
N	F_1	F_2	F_3	F_1	F_2	F_3	F_1	F_2	F_3
0	0.00			0.00			0.06		
1	0.00	0.00	0.00	0.04	0.25	0.25	0.02	0.31	0.56
2	0.00	0.00	0.00	0.07	0.43	0.00	0.19	0.05	0.10
3	1.02	0.10	0.01	0.55	0.92	0.04	0.10	0.30	0.53
4	2.48	0.55	0.06	0.46	1.73	0.53	0.02	0.39	1.82
5	−	0.84	0.00	1.00	*	2.36	0.00	3.31	*
6	0.92	0.07	0.00	0.02	1.04	1.01	0.02	0.32	1.04
7	0.08	0.00	0.00	0.10	0.07	0.13	0.14	0.00	0.18
8	0.00	0.00	0.00	0.00	0.00	0.07	0.01	0.00	0.01
	$\Sigma k=6.13$			$\Sigma k=11.07$			$\Sigma k=9.48$		

TABLE VIII. State-to-state rate constants $k_{He}^{(J,N)\to(J',N')}$ in units of 10^{-11} cm^3 molecule^{-1} s^{-1} for collision induced transitions with He as the collision partner. The accuracy of the single rate constants is 0.08 $\times 10^{-11}$ cm^3 molecule^{-1} s^{-1}, the accuracy of the sums is 0.4 $\times 10^{-11}$ cm^3 molecule^{-1} s^{-1}. The asterisk indicates initial levels which have been prepared in the experiment. All state-to-state rate constants with such an initial level are determined directly. The minus sign indicates initial levels which have not been prepared in the experiment. All rate constants with such an initial level are determined indirectly. The last row contains the sum of all rate constants which originate from the considered level indicated with an asterisk or a minus sign. $F_2(N=0)$ and $F_3(N=0)$ levels do not exist.

	Initial $N=7$ rate constants, collision partner He								
	Initial $N=7$, F_1			Initial $N=7$, F_2			Initial $N=7$, F_3		
N	F_1	F_2	F_3	F_1	F_2	F_3	F_1	F_2	F_3
0	0.00			0.02			0.02		
1	0.00	0.00	0.00	0.00	0.04	0.02	0.00	0.03	0.20
2	0.00	0.00	0.00	0.05	0.00	0.00	0.04	0.37	0.10
3	0.00	0.00	0.00	0.04	0.06	0.00	0.23	0.13	0.03
4	0.00	0.00	0.00	0.03	0.08	0.07	0.01	0.18	0.42
5	0.47	0.48	0.54	0.01	0.59	0.05	0.07	0.24	0.72
6	0.29	0.63	0.02	0.50	0.60	0.51	0.01	0.21	1.91
7	−	0.68	0.00	0.78	*	1.92	0.00	0.71	*
8	0.00	0.00	0.00	0.25	0.00	0.39	0.00	0.00	0.63
	$\Sigma k=3.11$			$\Sigma k=6.01$			$\Sigma k=6.26$		

-2.13 cm^3 molecule^{-1} s^{-1}] followed by the rate constants with F_1 [$\Delta(\Sigma k)/\Delta N=-1.90$ cm^3 molecule^{-1} s^{-1}] and F_2 [$\Delta(\Sigma k)/\Delta N=-1.77$ cm^3 molecule^{-1} s^{-1}] levels as the initial level. Here the total rate constant for the ($N=0$,F_1) level as the initial level is not taken into consideration because the ($N=0$,F_2) state for which the strongest transition probability would be expected does not exist. Total rate constants for N_2 as the collision partner behave similarly as in the case of He as the collision partner, but, the values are higher and the decrease $\Delta(\Sigma k)/\Delta N$ of the rate constants with a F_2 level as the initial level is stronger relative to the other rate constants. The situation in our previous study[8] where Ne was the collision partner is different. Here the rate constants with F_1 levels as the initial levels have the strongest decrease $\Delta(\Sigma k)/\Delta N$. The reason for the decrease of the total rate constants with increasing N is the increase of the energy spacing between the neighboring rotational levels and the typical strong dependence of the transferred energy in a collision.[26]

TABLE VII. State-to-state rate constants $k_{He}^{(J,N)\to(J',N')}$ in units of 10^{-11} cm^3 molecule^{-1} s^{-1} for collision induced transitions with He as the collision partner. The accuracy of the single rate constants is 0.08 $\times 10^{-11}$ cm^3 molecule^{-1} s^{-1}, the accuracy of the sums is 0.4 $\times 10^{-11}$ cm^3 molecule^{-1} s^{-1}. The asterisk indicates initial levels which have been prepared in the experiment. All state-to-state rate constants with such an initial level are determined directly. The minus sign indicates initial levels which have not been prepared in the experiment. All rate constants with such an initial level are determined indirectly. The last row contains the sum of all rate constants which originate from the considered level indicated with an asterisk or a minus sign. $F_2(N=0)$ and $F_3(N=0)$ levels do not exist.

	Initial $N=6$ rate constants, collision partner He								
	Initial $N=6$, F_1			Initial $N=6$, F_2			Initial $N=6$, F_3		
N	F_1	F_2	F_3	F_1	F_2	F_3	F_1	F_2	F_3
0	0.00			0.02			0.02		
1	0.00	0.00	0.00	0.01	0.02	0.03	0.00	0.02	0.39
2	0.00	0.00	0.00	0.03	0.01	0.00	0.04	0.00	0.40
3	0.00	0.00	0.00	0.24	0.35	0.00	0.00	0.28	0.67
4	0.00	0.38	0.00	0.15	0.75	0.04	0.03	0.28	0.78
5	2.02	0.03	0.03	0.18	1.51	0.45	0.00	0.27	1.23
6	−	0.70	0.00	0.81	*	1.53	0.00	1.70	*
7	0.11	0.17	0.00	0.28	0.10	0.49	0.01	0.00	0.73
8	0.00	0.00	0.00	0.00	0.00	0.00	0.05	0.00	0.08
	$\Sigma k=3.44$			$\Sigma k=7.00$			$\Sigma k=6.98$		

TABLE IX. State-to-state rate constants $k_{N_2}^{(J,N)\to(J',N')}$ in units of 10^{-11} cm^3 molecule^{-1} s^{-1} for collision induced transitions with N_2 as the collision partner. The accuracy of the single rate constants is 0.25 $\times 10^{-11}$ cm^3 molecule^{-1} s^{-1}, the accuracy of the sums is 1.2 $\times 10^{-11}$ cm^3 molecule^{-1} s^{-1}. The asterisk indicates initial levels which have been prepared in the experiment. All state-to-state rate constants with such an initial level are determined directly. The minus sign indicates initial levels which have not been prepared in the experiment. All rate constants with such an initial level are determined indirectly. The last row contains the sum of all rate constants which originate from the considered level indicated with an asterisk or a minus sign. $F_2(N=0)$ and $F_3(N=0)$ levels do not exist.

	Initial $N=0$, F_1 rate constants, collision partner N_2		
N	F_1	F_2	F_3
0	−		
1	20.00	8.75	0.94
2	11.24	7.66	0.64
3	4.72	0.77	0.69
4	1.80	0.29	1.56
5	0.00	0.09	0.06
6	0.00	0.00	0.10
7	0.00	0.00	0.02
8	0.00	0.00	0.00
	$\Sigma k=59.33$		

TABLE X. State-to-state rate constants $k_{N_2}^{(J,N)\to(J',N')}$ in units of 10^{-11} cm^3 molecule^{-1} s^{-1} for collision induced transitions with N_2 as the collision partner. The accuracy of the single rate constants is 0.25 $\times 10^{-11}$ cm^3 molecule^{-1} s^{-1}, the accuracy of the sums is 1.2 $\times 10^{-11}$ cm^3 molecule^{-1} s^{-1}. The asterisk indicates initial levels which have been prepared in the experiment. All state-to-state rate constants with such an initial level are determined directly. The minus sign indicates initial levels which have not been prepared in the experiment. All rate constants with such an initial level are determined indirectly. The last row contains the sum of all rate constants which originate from the considered level indicated with an asterisk or a minus sign. $F_2(N=0)$ and $F_3(N=0)$ levels do not exist.

	Initial $N=1$ rate constants, collision partner N_2								
	Initial $N=1$, F_1			Initial $N=1$, F_2			Initial $N=1$, F_3		
N	F_1	F_2	F_3	F_1	F_2	F_3	F_1	F_2	F_3
0	14.03			10.27			3.26		
1	*	3.82	2.37	4.73	*	1.96	11.81	5.82	–
2	12.24	1.73	0.49	5.18	10.35	3.75	19.46	7.83	7.44
3	3.92	2.41	0.32	1.06	1.24	0.32	9.16	4.44	5.20
4	0.71	0.49	0.09	0.50	0.53	0.07	1.73	1.44	2.11
5	0.00	0.16	0.07	0.19	0.23	0.07	0.00	0.61	0.91
6	0.19	0.06	0.01	0.00	0.01	0.01	0.00	0.10	0.28
7	0.15	0.01	0.00	0.07	0.00	0.00	0.00	0.04	0.04
8	0.04	0.01	0.00	0.04	0.01	0.02	0.00	0.00	0.00
	$\Sigma k=43.32$			$\Sigma k=40.61$			$\Sigma k=81.68$		

TABLE XII. State-to-state rate constants $k_{N_2}^{(J,N)\to(J',N')}$ in units of 10^{-11} cm^3 molecule^{-1} s^{-1} for collision induced transitions with N_2 as the collision partner. The accuracy of the single rate constants is 0.25 $\times 10^{-11}$ cm^3 molecule^{-1} s^{-1}, the accuracy of the sums is 1.2 $\times 10^{-11}$ cm^3 molecule^{-1} s^{-1}. The asterisk indicates initial levels which have been prepared in the experiment. All state-to-state rate constants with such an initial level are determined directly. The minus sign indicates initial levels which have not been prepared in the experiment. All rate constants with such an initial level are determined indirectly. The last row contains the sum of all rate constants which originate from the considered level indicated with an asterisk or a minus sign. $F_2(N=0)$ and $F_3(N=0)$ levels do not exist.

	Initial $N=3$ rate constants, collision partner N_2								
	Initial $N=3$, F_1			Initial $N=3$, F_2			Initial $N=3$, F_3		
N	F_1	F_2	F_3	F_1	F_2	F_3	F_1	F_2	F_3
0	4.02			0.85			1.06		
1	3.22	0.84	2.23	1.14	0.99	1.40	0.73	3.06	2.28
2	13.30	1.07	0.23	3.66	6.70	0.64	1.30	2.91	7.29
3	*	3.45	0.22	7.56	*	0.44	0.72	5.15	*
4	9.44	2.05	0.42	0.55	5.65	0.47	0.51	2.97	7.42
5	3.12	0.36	0.37	0.13	0.16	0.10	0.16	2.20	0.28
6	0.07	0.14	0.30	0.32	0.01	0.01	0.38	0.05	0.01
7	0.28	0.01	0.02	0.21	0.01	0.00	0.29	0.02	0.00
8	0.06	0.01	0.01	0.49	0.00	0.01	0.01	0.01	0.01
	$\Sigma k=45.24$			$\Sigma k=31.50$			$\Sigma k=38.82$		

Furthermore, in all studies including our study with Ne as the collision partner,[8] the total rate constant for transitions out of the initial level $(F_3, N=1)$ is extremely high (see Fig. 3). The mean total rate constants averaged over initial N, for He as the collision partner are $k_{F_1\to X}=8.16\times 10^{-11}$ cm^3 molecule^{-1} s^{-1}, $k_{F_2\to X}=11.95\times 10^{-11}$ cm^3 molecule^{-1} s^{-1} and $k_{F_3\to X}=11.81\times 10^{-11}$ cm^3 molecule^{-1} s^{-1} [where the total rate constant with the $(N=0,F_1)$ level as the initial level is not taken into consideration]. The mean total rate constant for F_2 levels as the initial level is the largest, similar to our previous study with Ne as a collision partner,[8] however, the error bars (1.2 $\times 10^{-11}$ cm^3 molecule^{-1} s^{-1}, see Tables I–VIII) overlap for $k_{F_2\to X}$ and $k_{F_3\to X}$ in this case. The reason is probably that generally collision induced transitions which change the spin component by ± 1 are the most effective collisions. Only transitions which originate from an F_2 level have two possibilities for such a transition, whereas

TABLE XI. State-to-state rate constants $k_{N_2}^{(J,N)\to(J',N')}$ in units of 10^{-11} cm^3 molecule^{-1} s^{-1} for collision induced transitions with N_2 as the collision partner. The accuracy of the single rate constants is 0.25 $\times 10^{-11}$ cm^3 molecule^{-1} s^{-1}, the accuracy of the sums is 1.2 $\times 10^{-11}$ cm^3 molecule^{-1} s^{-1}. The asterisk indicates initial levels which have been prepared in the experiment. All state-to-state rate constants with such an initial level are determined directly. The minus sign indicates initial levels which have not been prepared in the experiment. All rate constants with such an initial level are determined indirectly. The last row contains the sum of all rate constants which originate from the considered level indicated with an asterisk or a minus sign. $F_2(N=0)$ and $F_3(N=0)$ levels do not exist.

	Initial $N=2$ rate constants, collision partner N_2								
	Initial $N=2$, F_1			Initial $N=2$, F_2			Initial $N=2$, F_3		
N	F_1	F_2	F_3	F_1	F_2	F_3	F_1	F_2	F_3
0	7.70			7.37			1.02		
1	9.06	2.81	3.82	5.83	7.24	2.16	1.10	5.11	3.40
2	*	6.12	0.17	6.84	*	0.80	0.39	1.32	–
3	12.98	2.46	0.20	1.59	7.82	3.53	0.43	0.93	7.59
4	3.32	0.49	0.27	3.04	1.53	0.27	0.20	0.22	1.25
5	0.30	0.59	0.11	0.22	1.15	0.29	0.00	0.06	0.51
6	0.02	0.04	0.01	0.06	0.85	0.02	0.00	0.01	0.17
7	0.09	0.01	0.00	0.02	0.00	0.04	0.00	0.01	0.02
8	0.32	0.14	0.00	0.07	0.02	0.55	0.00	0.00	0.00
	$\Sigma k=51.03$			$\Sigma k=51.31$			$\Sigma k=23.74$		

TABLE XIII. State-to-state rate constants $k_{N_2}^{(J,N)\to(J',N')}$ in units of 10^{-11} cm^3 molecule^{-1} s^{-1} for collision induced transitions with N_2 as the collision partner. The accuracy of the single rate constants is 0.25 $\times 10^{-11}$ cm^3 molecule^{-1} s^{-1}, the accuracy of the sums is 1.2 $\times 10^{-11}$ cm^3 molecule^{-1} s^{-1}. The asterisk indicates initial levels which have been prepared in the experiment. All state-to-state rate constants with such an initial level are determined directly. The minus sign indicates initial levels which have not been prepared in the experiment. All rate constants with such an initial level are determined indirectly. The last row contains the sum of all rate constants which originate from the considered level indicated with an asterisk or a minus sign. $F_2(N=0)$ and $F_3(N=0)$ levels do not exist.

	Initial $N=4$ rate constants, collision partner N_2								
	Initial $N=4$, F_1			Initial $N=4$, F_2			Initial $N=4$, F_3		
N	F_1	F_2	F_3	F_1	F_2	F_3	F_1	F_2	F_3
0	2.34			0.46			3.20		
1	0.76	0.44	0.65	0.41	0.39	0.66	0.77	4.10	1.23
2	4.09	1.48	0.16	3.16	0.90	0.22	1.46	2.97	1.60
3	9.56	2.33	0.16	3.30	6.70	0.33	1.92	4.06	4.23
4	*	2.00	0.48	3.21	*	3.69	0.32	3.52	*
5	5.54	4.74	0.55	0.26	3.97	1.26	0.90	0.58	3.99
6	0.07	0.41	0.08	0.03	0.08	0.06	0.06	0.67	1.02
7	1.06	0.01	0.02	0.08	0.00	0.05	0.49	0.00	0.07
8	0.73	0.13	0.00	0.03	0.02	0.00	0.02	0.00	0.02
	$\Sigma k=37.79$			$\Sigma k=29.27$			$\Sigma k=37.20$		

TABLE XIV. State-to-state rate constants $k_{N_2}^{(J,N)\to(J',N')}$ in units of 10^{-11} cm^3 molecule^{-1} s^{-1} for collision induced transitions with N_2 as the collision partner. The accuracy of the single rate constants is 0.25 $\times 10^{-11}$ cm^3 molecule^{-1} s^{-1}, the accuracy of the sums is 1.2 $\times 10^{-11}$ cm^3 molecule^{-1} s^{-1}. The asterisk indicates initial levels which have been prepared in the experiment. All state-to-state rate constants with such an initial level are determined directly. The minus sign indicates initial levels which have not been prepared in the experiment. All rate constants with such an initial level are determined indirectly. The last row contains the sum of all rate constants which originate from the considered level indicated with an asterisk or a minus sign. $F_2(N=0)$ and $F_3(N=0)$ levels do not exist.

	Initial $N=5$ rate constants, collision partner N_2								
	Initial $N=5$, F_1			Initial $N=5$, F_2			Initial $N=5$, F_3		
N	F_1	F_2	F_3	F_1	F_2	F_3	F_1	F_2	F_3
0	0.00			0.25			0.22		
1	0.00	0.00	0.00	0.15	0.29	0.50	0.13	0.33	0.91
2	0.00	0.00	0.00	1.09	0.30	0.10	0.67	0.95	1.10
3	8.79	0.29	0.25	0.59	2.02	0.09	1.42	1.37	1.48
4	10.21	0.40	1.06	0.64	6.30	0.29	0.22	1.23	5.47
5	−	2.29	0.07	2.72	*	4.50	0.10	4.34	*
6	2.38	0.18	0.35	1.34	2.85	0.18	0.12	0.43	0.62
7	0.07	0.00	0.02	0.03	0.07	0.00	0.22	0.00	0.03
8	0.00	0.00	0.00	0.02	0.03	0.06	0.23	0.00	0.00
	$\Sigma k=26.36$			$\Sigma k=24.41$			$\Sigma k=23.59$		

TABLE XVI. State-to-state rate constants $k_{N_2}^{(J,N)\to(J',N')}$ in units of 10^{-11} cm^3 molecule^{-1} s^{-1} for collision induced transitions with N_2 as the collision partner. The accuracy of the single rate constants is 0.25 $\times 10^{-11}$ cm^3 molecule^{-1} s^{-1}, the accuracy of the sums is 1.2 $\times 10^{-11}$ cm^3 molecule^{-1} s^{-1}. The asterisk indicates initial levels which have been prepared in the experiment. All state-to-state rate constants with such an initial level are determined directly. The minus sign indicates initial levels which have not been prepared in the experiment. All rate constants with such an initial level are determined indirectly. The last row contains the sum of all rate constants which originate from the considered level indicated with an asterisk or a minus sign. $F_2(N=0)$ and $F_3(N=0)$ levels do not exist.

	Initial $N=7$ rate constants, collision partner N_2								
	Initial $N=7$, F_1			Initial $N=7$, F_2			Initial $N=7$, F_3		
N	F_1	F_2	F_3	F_1	F_2	F_3	F_1	F_2	F_3
0	0.00			0.11			0.39		
1	0.00	0.00	0.00	0.01	0.05	0.18	0.02	0.06	0.21
2	0.00	0.00	0.00	0.01	0.00	0.07	0.18	0.15	0.19
3	0.00	0.00	0.00	0.04	0.14	0.00	0.25	0.17	0.01
4	0.00	0.00	0.00	0.17	0.29	0.07	0.36	0.41	0.28
5	0.42	0.15	0.87	0.03	0.54	0.04	0.13	0.19	1.05
6	0.83	1.22	0.23	0.57	0.47	1.00	0.64	0.18	4.30
7	−	5.35	0.76	6.11	*	6.42	1.00	3.76	*
8	0.00	0.00	0.00	0.44	0.00	1.50	0.00	0.05	3.17
	$\Sigma k=9.83$			$\Sigma k=18.26$			$\Sigma k=17.15$		

transitions which originate from an F_1 or an F_3 level have only one such possibility. The situation for the mean total rate constants for transitions with N_2 as the collision partner is completely different. Here it is $k_{F_1\to X}=32.04\times 10^{-11}$ cm^3 molecule^{-1} s^{-1}, $k_{F_2\to X}=30.85\times 10^{-11}$ cm^3 molecule^{-1} s^{-1} (unexpectedly the lowest of the three values), and $k_{F_3\to X}=34.62\times 10^{-11}$ cm^3 molecule^{-1} s^{-1}. The rate constants with N_2 as the collision partner are about three times higher than those with He or Ne. This can be explained with the additional rotational degrees of freedom of the N_2 molecule.

For the state-to-state rate constants (Tables I–VIII for He as the collision partner and Tables IX–XVI for N_2 as the

TABLE XV. State-to-state rate constants $k_{N_2}^{(J,N)\to(J',N')}$ in units of 10^{-11} cm^3 molecule^{-1} s^{-1} for collision induced transitions with N_2 as the collision partner. The accuracy of the single rate constants is 0.25 $\times 10^{-11}$ cm^3 molecule^{-1} s^{-1}, the accuracy of the sums is 1.2 $\times 10^{-11}$ cm^3 molecule^{-1} s^{-1}. The asterisk indicates initial levels which have been prepared in the experiment. All state-to-state rate constants with such an initial level are determined directly. The minus sign indicates initial levels which have not been prepared in the experiment. All rate constants with such an initial level are determined indirectly. The last row contains the sum of all rate constants which originate from the considered level indicated with an asterisk or a minus sign. $F_2(N=0)$ and $F_3(N=0)$ levels do not exist.

	Initial $N=6$ rate constants, collision partner N_2								
	Initial $N=6$, F_1			Initial $N=6$, F_2			Initial $N=6$, F_3		
N	F_1	F_2	F_3	F_1	F_2	F_3	F_1	F_2	F_3
0	0.00			0.03			0.69		
1	0.00	0.00	0.00	0.05	0.05	0.18	0.09	0.07	0.58
2	0.00	0.00	0.00	0.08	0.00	0.05	0.20	0.05	0.76
3	0.00	0.00	0.00	0.26	1.50	0.03	0.10	0.87	1.62
4	0.30	0.10	0.17	0.36	2.45	0.08	0.10	0.97	1.60
5	5.24	2.49	0.18	0.45	4.48	0.47	1.07	0.20	4.63
6	−	1.51	0.05	1.75	*	5.50	0.07	3.35	*
7	0.32	0.19	0.19	0.54	0.24	1.97	0.12	0.04	2.97
8	0.00	0.00	0.00	0.02	0.02	0.05	0.00	0.00	0.00
	$\Sigma k=10.74$			$\Sigma k=20.61$			$\Sigma k=20.15$		

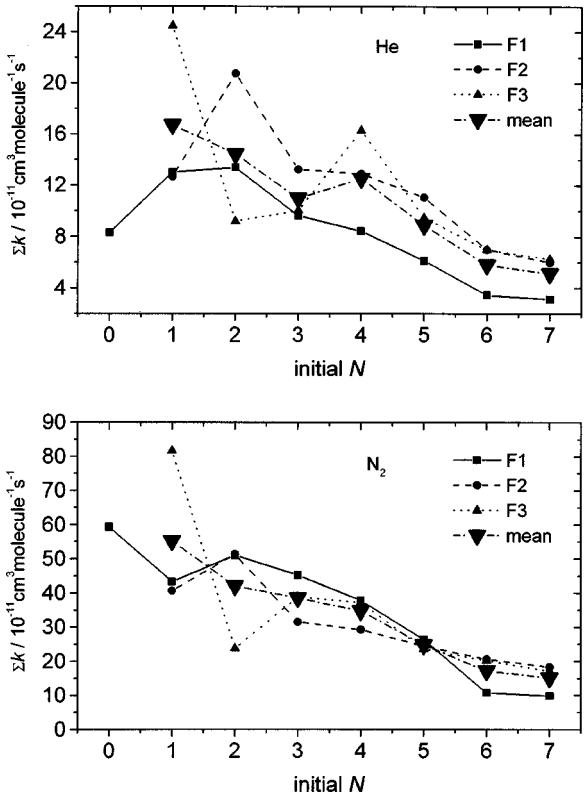

FIG. 3. Plot of the sum over all rate constants out of the (N,F_1), (N,F_2), and (N,F_3) states depending on the initial nuclear rotation quantum number N for He (upper part) and N_2 (lower part) as the collision partners. The numerical average value is indicated by "mean."

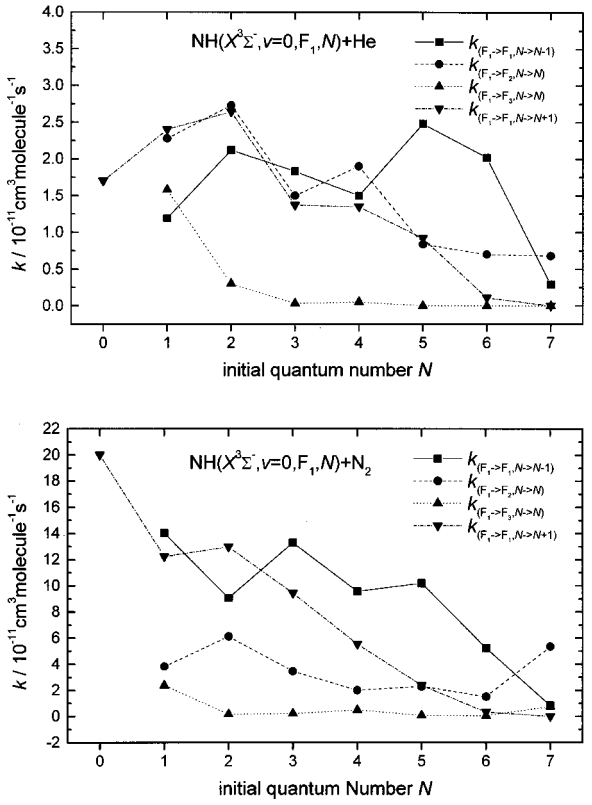

FIG. 4. State-to-state rate constants of collision induced transitions with He (upper part) and N_2 (lower part) with an F_1 level as the initial level and a neighboring level as the final level depending on the initial nuclear rotation quantum number N.

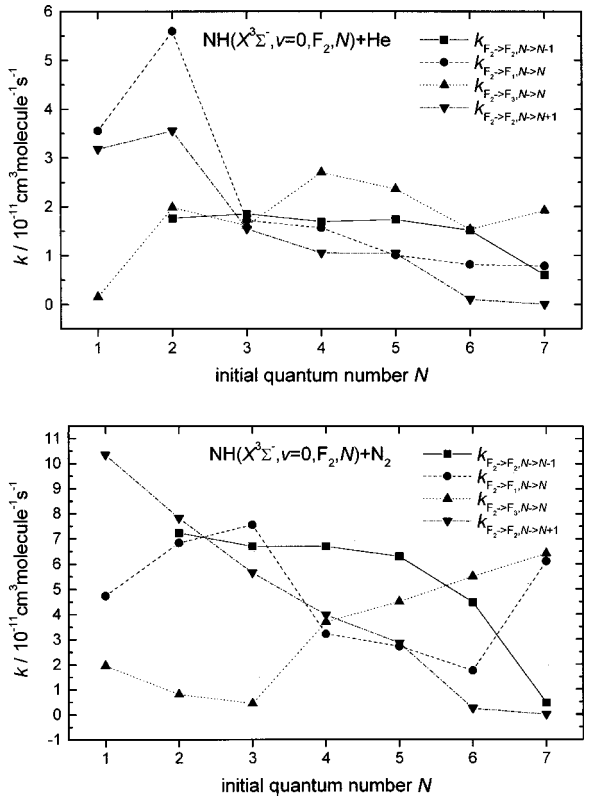

FIG. 5. State-to-state rate constants of collision induced transitions with He (upper part) and N_2 (lower part) with an F_2 level as the initial level and a neighboring level as the final level depending on the initial nuclear rotation quantum number N.

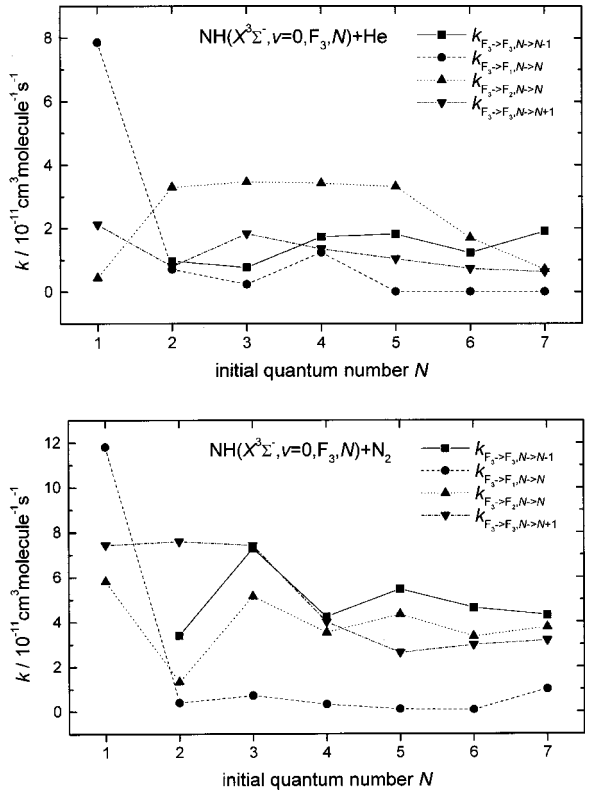

FIG. 6. State-to-state rate constants of collision induced transitions with He (upper part) and N_2 (lower part) with an F_3 level as the initial level and a neighboring level as the final level depending on the initial nuclear rotation quantum number N.

collision partner) generally the most effective transitions are transitions between neighboring levels. These are the rate constants where either the nuclear rotational quantum number N is changed by ± 1 or the index of the spin component i is changed by ± 1. If the spin component index i is changed by $\Delta i = \pm 2$ the rate constants are much lower. For collision induced transitions which occur within the same spin component we observe a regular behavior as is found in many other experiments described in the literature.[27] "Regular" means that there is a resonance for low transferred energies.

TABLE XVII. State-to-state rate constants in units of 10^{-11} cm^3 molecule^{-1} s^{-1} for collision induced transitions only considering the nuclear rotation quantum number N. The collision partner is He.

Final state N	Initial quantum state N							
	0	1	2	3	4	5	6	7
0	–	1.23	1.08	0.32	0.27	0.02	0.01	0.01
1	3.16	–	2.91	2.08	1.29	0.48	0.16	0.10
2	3.82	4.76	–	2.54	1.62	0.28	0.16	0.19
3	0.87	3.31	3.28	–	3.20	1.19	0.51	0.16
4	0.43	1.43	1.77	2.17	–	2.68	0.80	0.26
5	0.02	0.42	0.44	0.57	2.00	–	1.91	1.06
6	0.00	0.13	0.05	0.25	0.22	1.48	–	1.56
7	0.00	0.08	0.02	0.12	0.21	0.47	0.63	–
8	0.00	0.06	0.02	0.08	0.11	0.03	0.04	0.42

TABLE XVIII. State-to-state rate constants in units of 10^{-11} cm^3 molecule^{-1} s^{-1} for collision induced transitions only considering the nuclear rotation quantum number N. The collision partner is N_2.

Final state N	Initial quantum state N							
	0	1	2	3	4	5	6	7
0	–	9.28	5.36	1.98	2.00	0.16	0.24	0.17
1	29.69	–	13.51	5.30	3.14	0.77	0.34	0.18
2	19.54	22.82	–	12.37	5.35	1.40	0.38	0.20
3	6.18	9.36	12.51	–	10.86	5.43	1.46	0.20
4	3.65	2.56	3.53	9.83	–	8.61	2.04	0.53
5	0.15	0.75	1.08	2.29	7.26	–	6.40	1.14
6	0.10	0.22	0.39	0.43	0.83	3.48	–	3.15
7	0.02	0.10	0.06	0.28	0.59	0.15	2.19	–
8	0.00	0.04	0.37	0.20	0.32	0.11	0.03	1.72

Summing up, we find the following ''propensities'' for collision induced transitions with He and N_2 as the collision partner, similar to our previous study with Ne:[8]

$$\Delta N=0, \quad \Delta i=\pm 1, \tag{3}$$

$$\Delta N=\pm 1, \quad \Delta i=0. \tag{4}$$

Figure 4 represents a plot of the collision induced state-to-state rate constants for transitions between neighboring levels concerning N and i dependent on the initial N value for He as the collision partner (upper part of Fig. 4) and for N_2 as the collision partner (lower part of Fig. 4) with initial levels belonging to the F_1 spin component. Generally, the transition efficiency decreases with increasing N, agreeing well with a strong transition efficiency dependence on the transferred rotational energy ΔE. For the same reason the transitions $(F_1 \rightarrow F_1, N \rightarrow N-1)$ are more effective than the transitions $(F_1 \rightarrow F_1, N \rightarrow N+1)$. Exceptions are $N<3$ in the case of He and $N=2$ in the case of N_2. This is also the case for the analogous transitions within the other spin components (see Figs. 5 and 6). In the case of He and for quantum numbers $N>2$ the transitions $(F_1 \rightarrow F_1, N \rightarrow N-1)$ are the most effective transitions except for $N=4$ and $N=7$ whereas in the case of N_2 these transitions are the most effective ones except for $N=2$ and $N=7$. In the case of He these transitions have a local minimum of the efficiency at the quantum number $N=4$. For $N>1$ the transitions $(F_1 \rightarrow F_3, N \rightarrow N)$ with $\Delta i=2$ have the lowest efficiency for both He and N_2 due to violation of the propensities of Eqs. (3) and (4). For low N values the efficiency of those transitions rises slightly. This is similar to the case of Ne as the collision partner.[8]

Figure 5 shows the dependence of transitions between the neighboring rotational quantum states on the initial nuclear rotational quantum number N for initial levels within the F_2 spin component. For He as the collision partner (upper part of Fig. 5) the $(F_2 \rightarrow F_2, N \rightarrow N-1)$ transitions do not change significantly with increasing N and also the minimum at $N=4$ [see the analogous transition $(F_1 \rightarrow F_1, N \rightarrow N-1)$ in Fig. 4] is very weak. In the case of N_2 as the collision partner (lower part of Fig. 5) the minimum at $N=4$ does not exist at all. Here, the efficiency is very high for low N values decreasing monotonously. For $N=4$ and $N=5$ the $(F_2 \rightarrow F_2, N \rightarrow N-1)$ transitions are the strongest. For both He and N_2 the efficiency of the transition $(F_2 \rightarrow F_2, N \rightarrow N+1)$ is lower than the efficiency of the $(F_2 \rightarrow F_2, N \rightarrow N-1)$ transitions except for $N=2$. For the two possible spin component changing transitions $(F_2 \rightarrow F_1, N \rightarrow N)$ and $(F_2 \rightarrow F_3, N \rightarrow N)$ in all cases [including our study with Ne (Ref. 8)] for values $N>3$ the $(F_2 \rightarrow F_3, N \rightarrow N)$ transitions are more effective than the $(F_2 \rightarrow F_1, N \rightarrow N)$ transitions.

In Fig. 6 the rate constants of the transitions between the neighboring rotational quantum states with an F_3 state as the initial state are shown. Except for He, $N=3$ and N_2, $N<4$ the $(F_3 \rightarrow F_3, N \rightarrow N-1)$ transition is more effective than the $(F_3 \rightarrow F_3, N \rightarrow N+1)$ transition as is expected from the strong dependence on ΔE. Furthermore, in the case of He the $(F_3 \rightarrow F_2, N \rightarrow N)$ transition is most effective except for $N=1$ and $N=7$. For $N=7$ the $(F_3 \rightarrow F_3, N \rightarrow N-1)$ transition is the most effective one. In the case of N_2 and $N>3$ the $(F_3 \rightarrow F_3, N \rightarrow N-1)$ transition is most effective whereas for $N=3$ and $N=2$ the $(F_3 \rightarrow F_3, N \rightarrow N+1)$ transition is the most effective one. For both He (upper part of Fig. 6) and N_2 (lower part of Fig. 6), the $(F_3 \rightarrow F_1, N \rightarrow N)$ transition, which generally is very weak [due to violation of the propensity rule (3)], is the strongest transition for $N=1$ as the initial level. This unexpected result was also observed in our previous study with Ne.[8]

Previously, Dagdigian used a crossed beam apparatus to determine the relative cross sections for transitions out of the NH($X\ ^3\Sigma^-, v=0, J=1, N=0$) state by collisions with argon at a collision energy of 410 cm^{-1}.[28] Because of the fact that argon is a structureless target these state-to-state cross sections should be qualitatively comparable to the state-to-state rate constants we obtained for He in this work. The efficiency decreases with increasing N and the efficiency of transitions into levels which change the spin component more than one unit are ineffective. The results of Dagdigian are therefore in agreement with our observations and support our propensity rules.

Tables XVII and XVIII represent the state-to-state rate constants that result if only the nuclear rotation quantum number N is considered. The values are obtained by calculating the mean value of the rate constants of the three initial states (N,F_1), (N,F_2), and (N,F_3) and calculating the sum over the three final states (N',F_1), (N',F_2), and (N',F_3). First, collision induced transitions which change the nuclear rotation quantum number N by only ± 1 are clearly preferred. Second, there is a strong dependence on the initial nuclear rotational quantum number N. The rate constants for high initial N values are clearly smaller than the rate constants for low N values.

In order to quantify the dependence of the rate constants

TABLE XIX. Energy-gap law (EGL) parameters for collision induced transitions between different N states. The collision partner is He. a is in units of 10^{-11} cm^3 molecule^{-1} s^{-1}. β is dimensionless.

Initial N	0–7	0	1	2	3	4	5	6	7
a	0.62	2.28	0.98	1.08	0.69	0.92	1.82	0.17	0.11
Δa	0.1	0.8	0.3	0.5	0.3	0.6	0.6	0.2	0.1
β	1.18	2.88	1.19	1.56	1.21	1.32	0.42	0.72	0.38
$\Delta\beta$	0.1	0.3	0.1	0.2	0.2	0.3	0.1	0.6	0.2

TABLE XX. Energy-gap law (EGL) parameters for collision induced transitions between different N states. The collision partner is N_2. a is in units of 10^{-11} cm^3 molecule^{-1} s^{-1}. β is dimensionless.

Initial N	0–7	0	1	2	3	4	5	6	7
a	2.62	8.66	4.73	3.15	3.16	3.62	3.40	0.30	0.17
Δa	0.8	4.0	2.0	2.0	1.5	2.6	1.0	0.5	0.1
β	1.34	2.16	1.56	1.34	1.39	1.39	0.32	0.47	0.26
$\Delta\beta$	0.1	0.2	0.2	0.3	0.2	0.4	0.1	0.8	0.2

on the transferred energy, ΔE, the same procedure as for the case of Ne as the collision partner[8] is employed. The parameters of the energy-gap law (EGL) for vibrationally elastic collisions[29] are fitted to obtain the best agreement with the experimentally determined rate constants. It should be mentioned that the EGL just gives an overall impression of the rate constants as a function of energy. The EGL is not an exact representation of the individual rate constants. In the two-parameter version of the EGL a vibrationally elastic and rotationally inelastic rate constant is expressed by

$$k_{N\to N'}^{\mathrm{EGL}} = a(2N'+1)e^{(\beta\Delta E/kT)}, \tag{5}$$

where $\Delta E = |E_{N'} - E_N|$ represents the transferred energy and α and β are the two fit parameters. In order to obtain a linear form of Eq. (5) we first divide on both sides by the standard rate constant $k_0 = 10^{-11}$ cm^{-3} molecule^{-1} s^{-1} and then take the logarithm,

$$\ln\left(\frac{k_{N\to N'}^{\mathrm{EGL}}}{k_0(2N'+1)}\right) = \ln\left(\frac{a}{k_0}\right) - \beta\left(\frac{\Delta E}{kT}\right). \tag{6}$$

Using the scaling law in this form we perform a linear fit to our experimental data. Tables XIX and XX contain the results of this linear fit for He and N_2 as the collision partners. Furthermore, in order to obtain differential values for $\alpha(N)$ and $\beta(N)$ we also fitted the data separately for every single initial quantum number N. The results for these fits are also included in Tables XIX and XX. Figures 7 and 8 represent the plots of the linear fits for all initial quantum numbers N for He and N_2 as the collision partners. The general shape of the experimentally determined values indicates in both cases, He and N_2, that the EGL scaling law is suitable to describe the general dependence of the rate constants on the transferred energy ΔE. In Figs. 9 and 10 the plots of the linear fits for separate initial N values are shown. In general, the EGL scaling law is a good approximation of the rate constant dependence on the energy transfer, although individual k values might vary up to one order of magnitude.

IV. CONCLUSION

We completely state-selectively prepared NH radicals in their electronic and vibrational ground state ($X\,^3\Sigma^-, v=0, J, N$) using a new preparation technique[7] and extensively examined the state-to-state collision induced rotational energy transfer. We examined the collision induced change of the rotational quantum number N as well as the collision induced change of the spin component F_i. We presented state-to-state rate constants of collisions with He and N_2. In this work and in our previous work[8] state-to-state rotational energy transfer is examined for the first time within a molecular ground state.

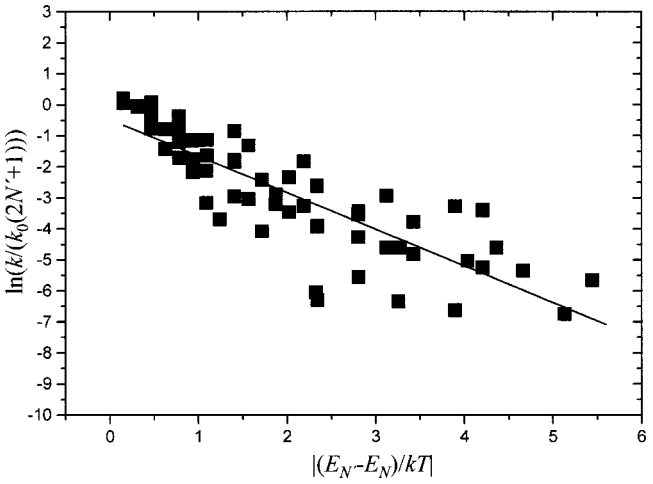

FIG. 7. Logarithmic energy-gap law (EGL) plot of ($N\to 0,1,...,8$) transitions with He as the collision partner. The straight line represents the linear fit that results in the obtained EGL constants. The plot shows that the energy-gap law describes the gross dependence of rate constants from the transferred energy. The deviation from the straight line is a property of each single collision induced transition and does not represent the experimental error which lies at 0.08 k_0.

Series of LIF spectra were recorded and fitted in order to determine the population distributions at different collision numbers of NH($X\,^3\Sigma^-, v=0, J, N$) molecules initially prepared in a single quantum state. The population data were modeled using smoothing spline functions, and state-to-state rate constants were calculated by an iterative algorithm integrating the population profiles.

As in our previous study[8] with Ne as the collision partner the rate constants obey the propensity rules

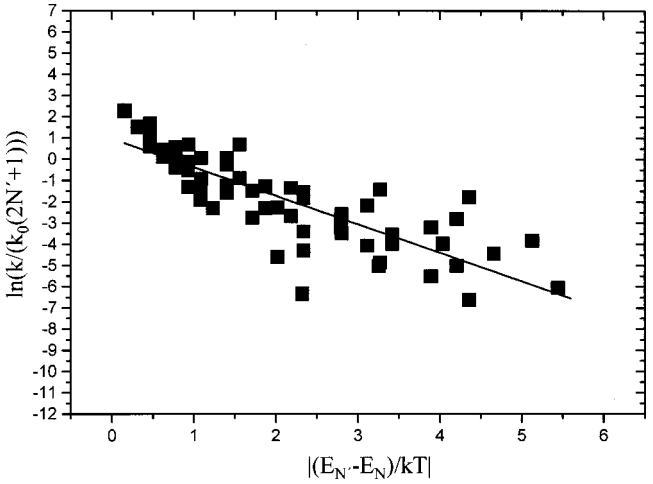

FIG. 8. Logarithmic energy-gap law (EGL) plot of ($N\to 0,1,...,8$) transitions with N_2 as the collision partner. The straight line represents the linear fit that results in the obtained EGL constants. The plot shows that also with N_2 as the collision partner the energy-gap law describes the dependence of rate constants from the transferred energy. The deviation from the straight line is a property of each single collision induced transition and does not represent the experimental error which lies at 0.25 k_0.

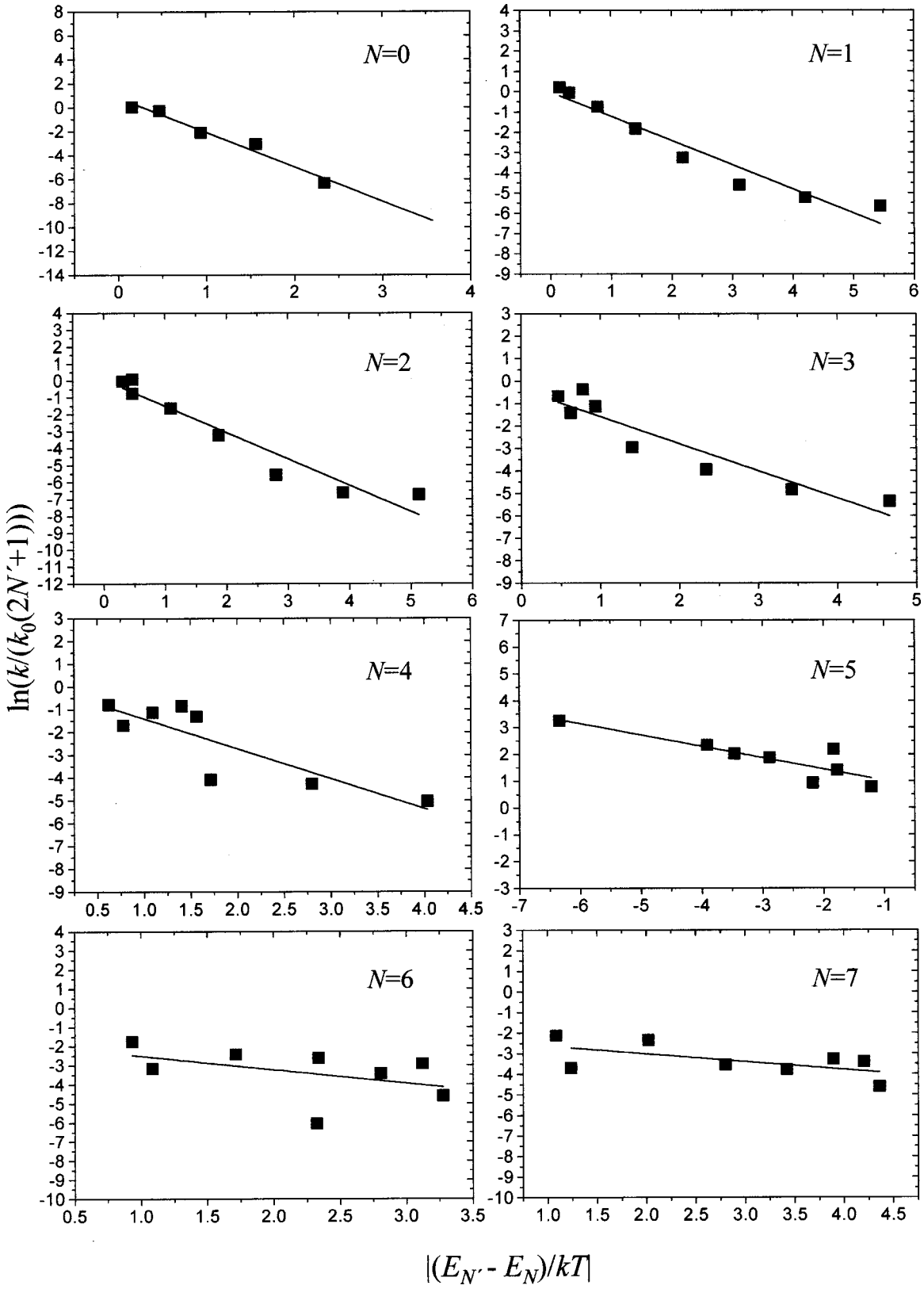

FIG. 9. Logarithmic energy-gap law (EGL) plots of ($N \rightarrow 0,1,...,8$) transitions with He as the collision partner separated for different initial N.

$$\Delta N = 0,\ \Delta i = \pm 1 \quad \text{and} \quad \Delta N = \pm 1,\ \Delta i = 0.$$

Thus usually collision induced transitions between neighboring levels are the most effective transitions.

The rate constants for N_2 as the collision partner are three times higher than the rate constants for He. Generally, the transition efficiency decreases with increasing N. However, the total rate constant for transitions out of the initial

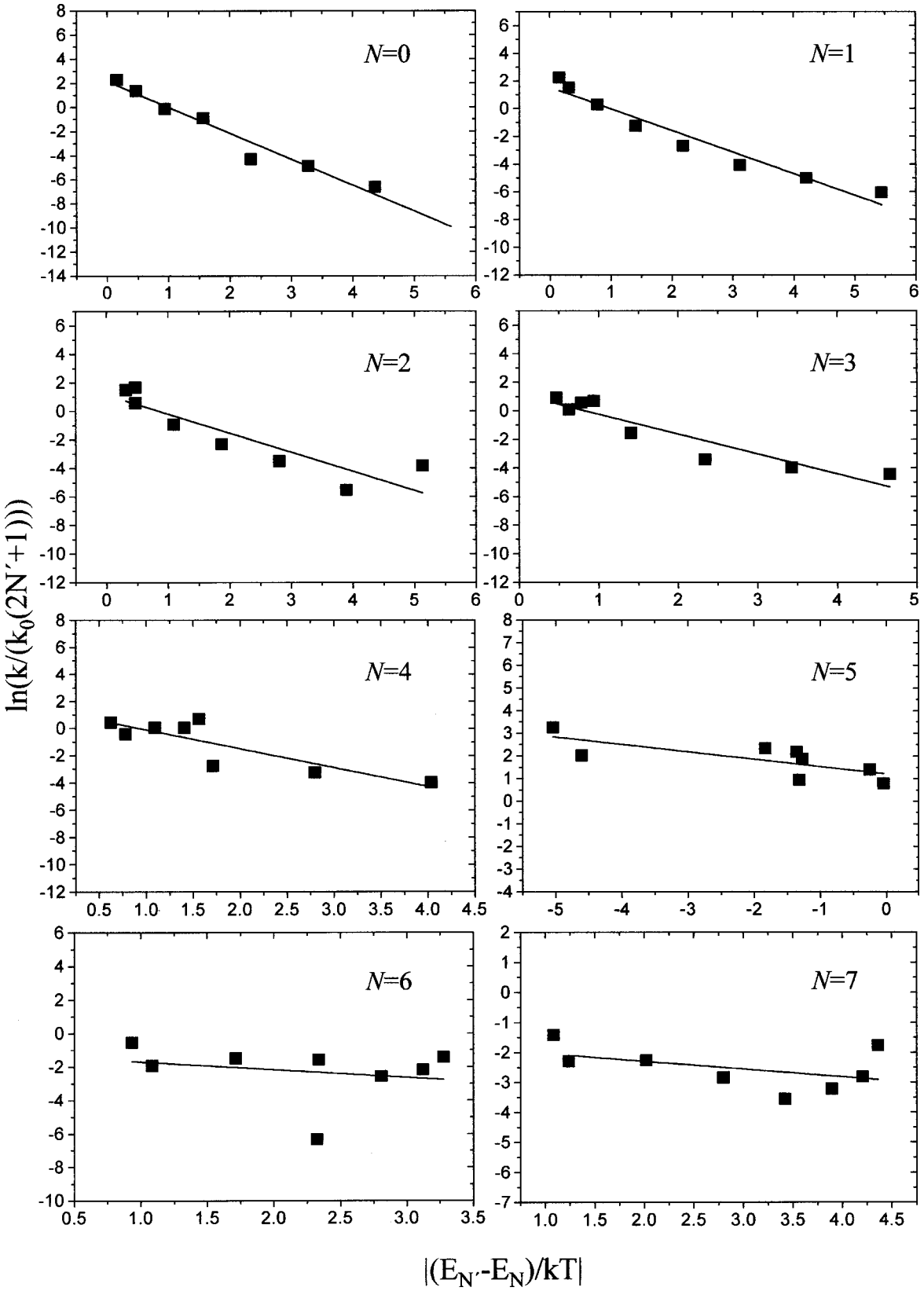

FIG. 10. Logarithmic energy-gap law (EGL) plots of ($N\rightarrow 0,1,\ldots,8$) transitions with N_2 as the collision partner separated for different initial N.

level ($F_3, N=1$) is extremely high. Surprisingly, for He and N_2 as the collision partners the transition ($F_3\rightarrow F_1, N=1 \rightarrow N=1$) is the strongest of all transitions with an F_3 level as the initial level.

($N\rightarrow N'$) rate constants, which only consider the change in the nuclear rotation quantum number, were extracted from the state-to-state rate constants by calculating the mean values concerning the three initial spin components and taking

the sum over the three final spin components. The detailed dependence of the $(N \rightarrow N')$ rate constants on the transferred energy is examined by fitting the experimental data to a two parameter version of the energy-gap law (EGL) for vibrationally elastic collisions.[29] EGL parameters for every single initial quantum number N are calculated. The EGL parameters are different for very initial quantum number N and the resolved state-to-state rate constants $(J,N \rightarrow J'N')$, from which the $(N \rightarrow N')$ rate constants are calculated, vary tremendously. Nevertheless, the EGL well describes the values of the rate constants. Thus the rate constant behavior concerning the transferred energy and implicitly the quantum number N is regular.

The experimentally determined rate constants are tremendously important because they allow the solution of the master equation (1) for chemical transformations that occur in nature around several hundred kelvin where small molecules are in the electronic and vibrational ground state. Additionally, the data (especially for He as a collision partner because it has only two electrons) are of great value for the theory of collision dynamics because they represent a benchmark for the theoretical treatment of collisions involving $X\ ^3\Sigma^-$ states of molecules.

ACKNOWLEDGMENTS

Financial support of this work by the Deutsche Forschungsgemeinschaft and Fonds der Chemischen Industrie is gratefully acknowledged. The authors thank C. Maul for valuable comments on the manuscript.

[1] P. J. Dagdigian, J. Chem. Phys. **90**, 6110 (1989).
[2] K. Schreel, J. Schleipen, A. Eppink, and J. J. ter Meulen, J. Chem. Phys. **99**, 8713 (1993).
[3] J. A. Mack, K. Mickulecky, and A. M. Wodke, J. Chem. Phys. **105**, 4105 (1996), and Refs. 1–18 therein.
[4] A. Kaes and F. Stuhl, J. Chem. Phys. **97**, 4661 (1992).
[5] M. Yang, M. H. Alexander, H.-J. Werner, J. Hohmann, L. Neitsch, F. Stuhl, and P. J. Dagdigian, J. Chem. Phys. **102**, 4069 (1995).
[6] L. Neitsch, F. Stuhl, P. J. Dagdigian, and M. H. Alexander, J. Chem. Phys. **104**, 1325 (1996).
[7] J. L. Rinnenthal and K.-H. Gericke, J. Chem. Phys. **111**, 9465 (1999).
[8] J. L. Rinnenthal and K.-H. Gericke, J. Chem. Phys. **113**, 6210 (2000).
[9] I. Glassman, *Combustion* (Academic, New York, 1977), p. 219.
[10] G. B. Debrou, J. M. Goodings, and D. K. Bohme, Combust. Flame **39**, 1 (1980).
[11] J. L. Rinnenthal and K.-H. Gericke, J. Mol. Spectrosc. **198**, 115 (1999).
[12] F. Freitag, F. Rohrer, and F. Stuhl, J. Phys. Chem. **93**, 3170 (1989).
[13] R. D. Bower, M. T. Jacoby, and J. A. Blauer, J. Chem. Phys. **86**, 1954 (1987).
[14] T. Haas, K.-H. Gericke, and C. Maul, Chem. Phys. Lett. **202**, 108 (1993).
[15] M. Hawley, A. P. Baronavski, and H. H. Nelson, J. Chem. Phys. **99**, 2638 (1993).
[16] K.-H. Gericke, T. Haas, M. Lock, R. Theinl, and F. J. Comes, J. Phys. Chem. **95**, 6104 (1991).
[17] (unpublished).
[18] I. Kovacs, *Rotational Structure in the Spectra of Diatomic Molecules* (Hilger, London, 1969), p. 181.
[19] P. W. Fairchild, G. P. Smith, D. R. Crosley, and J. B. Jeffries, Chem. Phys. Lett. **107**, 181 (1984).
[20] J. M. Eder, Denkschr. Wien. Akad. **60**, 1 (1893).
[21] G. W. Funke, Z. Phys. **96**, 787 (1935).
[22] R. N. Dixon, Can. J. Phys. **37**, 1171 (1959).
[23] J. Malicet, J. Brion, and H. Guenebaut, J. Chim. Phys. **67**, 25 (1970).
[24] C. R. Brazier, R. S. Ram, and P. F. Bernath, J. Mol. Spectrosc. **120**, 381 (1986).
[25] R. S. Ram, P. F. Bernath, and K. H. Hinkle, J. Chem. Phys. **110**, 5557 (1999).
[26] N. C. Lang, J. C. Polanyi, and J. Wanner, Chem. Phys. **24**, 219 (1977).
[27] R. D. Levine and R. B. Bernstein, *Molecular Reaction Dynamics and Chemical Reactivity* (Oxford University Press, New York, 1987).
[28] P. J. Dagdigian, J. Chem. Phys. **90**, 6110 (1989).
[29] J. I. Steinfeld and P. Ruttenberg, "Tests of Scaling Laws for Inelastic Collision Processes in Diatomic Halogen Molecules," Report No 23, Atomic Collisions Data Center, Joint Institute for Laboratory Astrophysics, Boulder, CO, 1983.